ACS OMEGA

Article

Cite This: ACS Omega 2019, 4, 19772−19776

http://pubs.acs.org/journal/acsodf

Electrochemical Deposition of Conformal Semiconductor Layers in Nanoporous Oxides for Sensitized Photoelectrodes

Jae Hyun Park,[†] Qing Wang,[§] Kai Zhu,[∥] Arthur J. Frank,*[,∥] and Jin Young Kim*[,†,‡]

[†]Department of Materials Science and Engineering and [‡]Research Institute of Advanced Materials (RIAM), Seoul National University, Seoul 08826, Republic of Korea

[§]Department of Materials Science and Engineering, Faculty of Engineering, National University of Singapore, Singapore 117576

[∥]National Renewable Energy Laboratory, Golden, Colorado 80401, United States

ABSTRACT: Nanoporous photoelectrodes with photoactive semiconductors have been investigated for various energy applications such as solar cells and photoelectrochemical cells, but the deposition of the semiconducting materials on the nanoporous electrodes has been very challenging due to pore clogging or complete pore filling. Here, we propose a band alignment model that explains the morphology of the electrochemically deposited semiconductor layer on the semiconducting nanoporous oxide electrode. Briefly, the coating material with a conduction band edge higher (i.e., more negative) than that of the electrode material forms a conformal coating, which maintains the initial nanoporous structure. As a result, a conformal CdSe layer can be electrodeposited onto TiO_2 nanotubes, which can be used as a photoelectrode of a sensitized solar cell. The electron dynamics studies revealed that the CdSe-sensitized TiO_2 nanotube electrode exhibited faster charge transport and slower charge recombination than its dye-sensitized counterpart, which has been ascribed to the passivation of surface traps and the physically blocked back-electron transfer by the CdSe layer as well as the higher conduction band of CdSe.

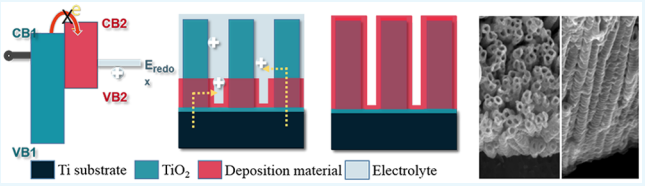

1. INTRODUCTION

Sensitized solar cells (SSCs) with various sensitizers including molecular dyes,[1,2] quantum dots,[3−5] and thin inorganic layers[6] have attracted much attention as potential candidates for next-generation low-cost modestly efficient solar cell devices. Among the sensitizers, the thin inorganic layers possess advantages of prominent light absorption capability,[7] tunable electronic properties,[8] and direct deposition on the oxide electrodes over other sensitizers.[9] A typical thin inorganic layer SSC consists of an electron-transporting phase, a sensitizer, and a hole-transporting phase. The electron-transporting phase is typically a nanoporous oxide semiconductor where the pores are generally less than 100 nm for obtaining larger surface area. The sensitizer covers the surface of the electron-transporting nanostructure. The liquid or solid hole-transporting phase is infiltrated into the pores of the sensitized electron-transporting electrode. Therefore, it is critical to maintain the nanoporous structure after depositing the sensitizer to obtain a typical SSC structure.

The electrochemical deposition has been one of the most popular processes to fabricate inorganic thin films[10,11] and to fill the pores of electrically insulating nanostructures like porous aluminum oxide films.[12] However, it has been challenging to control the morphology of deposited materials within nanoporous semiconducting electrodes (e.g., TiO_2 electron-transporting electrodes of SSCs) owing to the small pore size and electrical conductivity of the electrode materials. For instance, it has been shown that the semiconductors usually do not fill the pores of the electrodes but form an overlayer on top of the electrodes owing to the predominant deposition at the entrance of the pores.[13] One approach to overcome this clogging issue has been demonstrated by filling the pores with the deposition electrolyte followed by the electrochemical deposition in an inert electrolyte.[13] We previously developed a general electrochemical bottom-up growth approach by adjusting the ambipolar diffusion length (characteristic reaction length) by controlling the ionic strength of the electrolyte sovlent[14] where the bottom-up growth of p-type $CuInSe_2$ (CIS) in ordered nanoporous n-type TiO_2 electrodes was demonstrated. In the same study, we also showed that CIS completely filled the entire TiO_2 pore structure. However, for the traditional SSC structure, a conformal coating of the inorganic sensitizer is required to ensure the open pore structure. A couple of papers[15,16] reported the electrochemical deposition of the conformal CdSe or CdTe layer on the surface of ZnO nanowire arrays having average diameters/pores of hundred nanometers where the pores are interconnected to each other. On the other hand, there has been no report on the electrochemical deposition of conformal semiconductor layers on the electrically conducting nanoporous network with isolated pores less than 100 nm. Furthermore, no mechanistic study has been reported regarding the factors determining the deposition morphology

Received: August 9, 2019
Accepted: October 30, 2019
Published: November 13, 2019

DOI: 10.1021/acsomega.9b02552
ACS Omega 2019, 4, 19772−19776

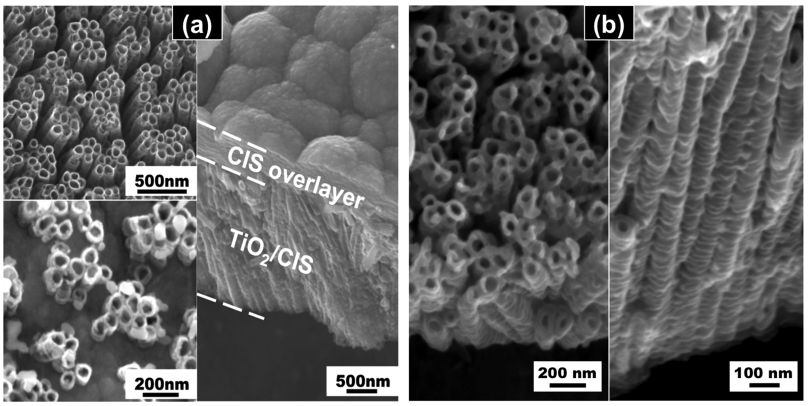

Figure 1. (a) SEM images of CIS-deposited TiO_2 NT arrays, showing a complete bottom-to-up pore filling behavior (upper left: before deposition; lower left: during the deposition (2.9 h); right: overlayer formation after a 3.8 h deposition at −0.95 V vs Ag/AgCl). Note that panel (a) was adopted from our previous publication.[14] (b) SEM images of CdSe-coated TiO_2 NT arrays where CdSe was coated conformally on the surface of TiO_2 NTs after 43200 pulse cycles (i.e., 6 h of deposition at −0.85 V vs Ag/AgCl).

between the complete pore filling and the conformal coating within a nanoporous semiconductor network.

In this study, we propose a band alignment model that determines whether a semiconductor would fill the pores of the semiconducting oxide electrode completely or it would form a conformal coating on the surface of the electrode by electrochemical deposition. As a proof-of-concept example of this model, we discuss the results of CdSe deposition on the TiO_2 nanotube (NT) arrays, and its growth behavior was compared with that of the CIS/TiO_2 NT counterpart. The interfacial charge transfer between the host nanoporous electrode and the coating material is found to be affected by the relative position of their conduction band edge, which in turn determines the deposition morphology (i.e., conformal coating vs pore filling). For example, we found that the conduction band offset between TiO_2 and as-deposited CdSe results in the conformal coating of CdSe on TiO_2 NT arrays. Also, the electron transport and recombination properties of the CdSe-sensitized solar cell (CdSe-SSC) consisting of the conformal CdSe-coated TiO_2 NT arrays were compared with those of its conventional dye-sensitized counterpart (DSSC). At a fixed photoelectron density, the CdSe-SSC with a cobalt-based electrolyte system exhibit 10 times faster transport and 2 times slower recombination than the DSSC with the same electrolyte.

2. EXPERIMENTAL SECTION

2.1. TiO_2 Nanotube Preparation. Oriented TiO_2 NT arrays were prepared by electrochemically anodizing Ti foil (Alfa, 0.25 mm, 99.5% purity) in a two-electrode cell with a Pt counter electrode. The anodization electrolyte consisted of 0.15 M ammonium fluoride (Aldrich, 99.9%) and 3.5 wt % water in formamide (Aldrich, 99.9%). The Ti foils were biased at 20 V for 2 h at room temperature, resulting in 2 μm thick amorphous NT arrays. As-prepared NT films were rinsed with water and ethanol followed by the subsequent thermal crystallization at 400 °C in air for 1 h.

2.2. CdSe Deposition. The electrochemical deposition was carried out using a computer-controlled potentiostat (EG&G, PAR283) with a three-electrode cell with a Pt mesh counter electrode and a Ag/AgCl quasi-reference electrode (calibrated against $[Fe(CN)_6]^{3-/4-}$). The CdSe was deposited on the TiO_2 NT electrode by a potential pulse method (−0.85 V vs Ag/AgCl for 0.5 s and open circuit for 2.5 s) with a deposition solution composed of 20 mM $CdCl_2$ (Aldrich, 99.99%) and 4 mM H_2SeO_3 (Aldrich, 99.999%) in absolute ethanol (Pharmco-Aaper, 200 prf). After deposition, CdSe was crystallized by annealing at 400 °C for 1 h (ramp rate of 5 K·min^{-1}) under a N_2 atmosphere.

2.3. Thin Absorber Solar Cell. CdSe-coated TiO_2 NT films were assembled into sensitized solar cells according to the procedure described in our previous paper.[17] Briefly, the device was assembled in a sandwich configuration with the nanotube film facing a counter electrode, prepared by spreading a droplet of 5 mM H_2PtCl_6 in 2-isopropanol onto the commercial F:SnO_2 (FTO, TEC15) conducting glass substrate and subsequently firing it at 350 °C. In order to prepare the electrolyte solution, 0.2 M $[Co(phen)_3](ClO_4)_2$ (tris[1,10-phenanthroline]cobalt(II) perchlorate), 0.02 M Co^{3+} complex ($[Co(dtb\text{-}bpy)_3](ClO_4)_3$, tris[4,4′-di-*tert*-butyl-2,2′-bipyridine]cobalt(III) perchlorate),[18] and 0.2 M $LiClO_4$ were dissolved in the mixture solvent composed of acetonitrile and ethylene carbonate (4:6 in volume ratio). The Co^{3+} complex was used instead of the chemical oxidizing agents like $NOBF_4$ (nitrosodium tetrafluoroborate) to prevent the possible production of nitric oxide (NO) species.[19] The active area after cell assembly was 0.5 cm^2.

2.4. Characterization. The crystalline structure and microstructure of the CdSe-coated TiO_2 NT films were characterized by X-ray diffraction (XRD) and field-emission scanning electron microscopy (FE-SEM). Transport and recombination properties were measured by intensity-modulated photocurrent spectroscopy and intensity-modulated photovoltage spectroscopy as described previously.[20] For these measurements, the solar cells were probed with a modulated beam of 680 nm light superimposed on a relatively large background (bias) illumination, also at 680 nm. The probe and bias light entered the cell from the counter electrode side.

3. RESULTS AND DISCUSSION

As described in the Introduction, our previous study revealed that the CIS completely fills the pores of TiO_2 NT arrays during the electrochemical deposition.[14] As a result, the sample forms a very nice p−n bulk heterojunction structure (Figure 1a). However, the conduction band edge position of CIS (+0.2 eV vs NHE)[21] is lower than that of TiO_2 (−0.5 eV vs NHE),[22] hindering efficient injection of photoelectrons from CIS to

DOI: 10.1021/acsomega.9b02552
ACS Omega 2019, 4, 19772−19776

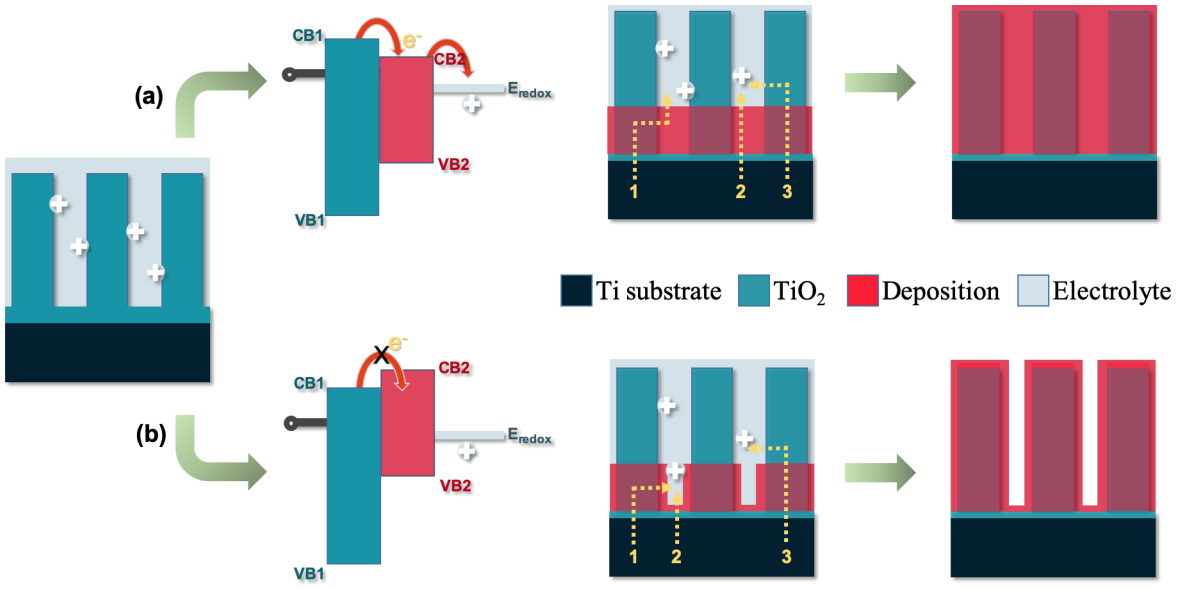

Figure 2. Schematic bottom-up deposition mechanisms for (a) complete pore filling and (b) conformal coating.

TiO_2, which is not ideal for a p−n bulk heterojunction solar cell. So, we selected CdSe as an alternative to CIS because its conduction band edge position (−0.8 eV vs NHE)[23] is known to be higher than that of TiO_2, and thus, the photoelectrons can be easily injected to TiO_2.[24] One could expect a similar p−n bulk heterojunction structure with CdSe if the same electrochemical deposition technique were used. However, as shown in Figure 1b, the morphology of CdSe after the electrochemical deposition was totally different from that of CIS. CdSe forms a conformal coating on the nanoporous TiO_2 NT arrays, resulting in a porous structure that is suitable for a conventional three-phase sensitized solar cell. Comparing the NT morphology before and after the deposition (i.e., upper left image in Figure 1a and lower left image in Figure 1b, NT walls get thicker after CdSe deposition, but pores are still open throughout the NT. The analysis of SEM images with higher magnifications (not shown) revealed that the thickness of the NT walls increases from 10−15 to 20−25 nm, whereas the inner diameter of the NT pores decreases from 60−70 to 50−60 nm. This result indicates that the conformal CdSe layer with a thickness of ∼5 nm covers both inner and outer surfaces of the NTs. So, what mechanism during the electrochemical deposition allows CdSe to form a conformal layer as opposed to the complete pore filling by CIS? Given the reason why we chose CdSe as opposed to CIS (i.e., conduction and edge positions), we hypothesized that the band alignment between the host n-type electrode and guest p-type semiconductor materials would affect the behavior of the electrochemical deposition.

Figure 2 shows a schematic illustration of the effects of the in situ band alignment between the electrode and as-deposited coating materials on the final deposition morphology. During the cathodic electrochemical deposition using a negative bias potential, the electrons needed for the deposition (i.e., the reduction of the reactants) should be supplied from the conducting substrate to the electrode/electrolyte interface. It is noteworthy that all the deposition mechanisms in this study were discussed assuming that the solvent with a low ionic strength like the absolute ethanol was used for the deposition. With such a solvent, the ambipolar diffusion length of the electrons in the nanoporous TiO_2 electrode filled with the electrolyte is sufficiently short, resulting in the bottom-up growth.[14] In the case where the conduction band edge of the coating material is lower (i.e., more positive) than that of the electrode material (Figure 2a), the electron transfer from the electrode to the coating layer is facilitated due to the appropriate band alignment. Therefore, the deposition takes place at both the coating material/electrolyte interface (routes 1 and 2 in panel (a)) and the nearby electrode/electrolyte interface (route 3 in panel (a)), resulting in the complete filling of the pores with the coating material. On the other hand, if the conduction band position of the coating material is higher (i.e., more negative) than that of the electrode material, the electron transfer from the electrode to the coating layer is obstructed by the inappropriate band alignment. In this case, deposition will stop once the electrode surface is covered by the coating layer with a certain thickness (routes 2 and 3 in panel (a)), causing electrons to migrate further through the electrode to find a suitable reaction site (i.e., the electrode/electrolyte interface; route 1 in panel (a)). Consequently, the coating layer will grow conformally on the electrode surface from bottom to top. This model can also explain the conformal coating of CdSe on the nanoporous ZnO film reported by other groups.[15,25] Indeed, ZnO and TiO_2 are known to have very similar conduction band levels, as well as valence band positions and band gap values,[26] which results in similar band alignments with CdSe.

Figure 3a shows the XRD patterns of a CdSe-coated TiO_2 NT film before and after annealing at 400 °C under a N_2 atmosphere. The as-deposited CdSe is amorphous, as no peak other than crystalline anatase peaks (denoted as A) from the TiO_2 NTs and Ti metal peaks (denoted as *) can be observed. The XRD pattern of the TiO_2 NT electrode (i.e., the as-deposited sample) is consistent with previous reports on anodized TiO_2 NT systems.[27,28] After annealing, the as-deposited amorphous CdSe layer was crystallized to the hexagonal wurtzite structure with characteristic three peaks between 23 and 28° (with a CuKα radiation) denoted as C. Because the as-deposited CdSe layer is amorphous, the in situ band alignment between CdSe and TiO_2 that was assumed

DOI: 10.1021/acsomega.9b02552
ACS Omega 2019, 4, 19772−19776

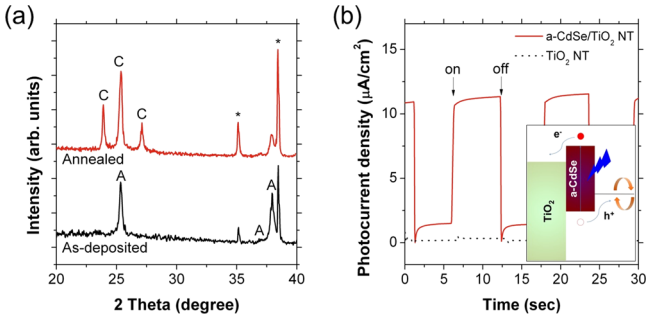

Figure 3. (a) X-ray diffraction patterns of CdSe-coated TiO_2 NT arrays before and after annealing at 400 °C for 1 h under a N_2 atmosphere where C, A, and the asterisk (*) indicate peaks of CdSe (wurtzite, JPCDS #77-2307), TiO_2 (anatase, JPCDS #21-1272), and Ti metal substrate (JPCDS #44-1294), respectively. (b) Photocurrent density profiles of TiO_2 NT electrodes with and without the as-deposited CdSe layer under pulse illumination by 470 nm light where the inset shows an illustration of the band alignment and the resulting charge injection between the as-deposited CdSe layer and the TiO_2 NT.

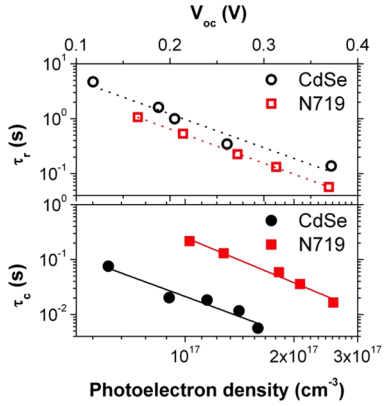

Figure 4. Transport time constants (τ_c, solid symbols) as a function of photoelectron density and recombination time constants (τ_r, open symbols) as a function of open circuit photovoltage (V_{oc}) for CdSe-sensitized (circles) and N719-dye-sensitized (squares) TiO_2 NT solar cells where the solid/dotted lines show the best fit of the data.

based on the conduction band position of crystalline CdSe has to be confirmed. Figure 3b compares the photoresponse of the TiO_2 NT electrodes in the presence and in the absence of the as-deposited CdSe, from which one can determine the in situ band alignment between CdSe and TiO_2 during the deposition. A three-electrode electrochemical setup similar to the electrochemical deposition was used with an aqueous polysulfide electrolyte (0.1 M Na_2S, 0.1 M S, and 0.1 M NaOH). A blue-light-emitting diode with a characteristic wavelength of 470 (±10) nm (i.e., 2.64 eV) and an optical power of 5 mW was used as a visible-light source. Given the estimated band gap energy of each material (i.e., 1.72 eV for CdSe and 3.2 eV for TiO_2), it was assumed that most incident photons would be absorbed by CdSe. For better comparison, the lowest current during the pulse illumination was set to zero. It is evident from the difference between the two current density profiles that the as-deposited CdSe is photoactive and the excited photoelectrons are being injected to the TiO_2 conduction band as illustrated in the inset of Figure 3b. If the conduction band edge of the as-deposited CdSe were lower than that of TiO_2, no photocurrent should have been observed from this measurement. The direction of the photocurrent (i.e., anodic photocurrent), which was confirmed by comparing to that of a normal dye-sensitized solar cell, also supports the band alignment assumption between as-deposited CdSe and TiO_2.

Figure 4 shows the transport (τ_c) and recombination (τ_r) time constants for a CdSe-sensitized TiO_2 NT solar cell (CdSe-SSC) and a dye-sensitized counterpart (DSSC), both of which use a cobalt-based electrolyte system. Both τ_c and τ_r exhibit the usual power-law dependency on photoelectron density and V_{oc}, respectively. The power-law dependency of τ_c can be explained by a model in which electrons perform an exclusive random walk between trap sites that have a power-law distribution of waiting (release) times in the form of $t^{-1-\alpha}$, where parameter α is in the range from 0 to 1 and can be related to the shape of the trap distribution.[29,30] From the best fits of the τ_c data in Figure 4 to the expression τ_c ($\propto D_n^{-1}$) $\propto n^{1-1/\alpha}$,[31] the respective α values for the CdSe-SSC and the DSSC were determined to be 0.29 and 0.27, respectively. Similar α values are understandable, as the two solar cells consist of the same electron-transporting phase (i.e., the TiO_2 NT arrays). At a given photoelectron density or V_{oc} (i.e., the same quasi-Fermi level), the CdSe-SSC exhibits 10 times faster transport and 2 times slower recombination than the DSSC, which should lead to a much higher charge-collection efficiency (η_{cc}). The slower recombination of the CdSe-SSC than the DSSC can be attributed to the existence of the CdSe conformal layer, which can physically/energetically prevent the electron recombination from TiO_2 to the oxidized electrolyte species. The faster electron transport in the CdSe-SSC is also likely associated with the changes of the surface properties. Passivation of surface traps by the conformal CdSe layer could lead to faster electron transport, owing to the reduced number of traps that the electrons visit and thus the reduced time that the electrons spend before they are collected by the Ti foil.[32] In addition, the conduction band offset at the CdSe/TiO_2 interface could confine the injected electrons in the region relatively far from the TiO_2 surface, which should similarly result in faster transport.

4. CONCLUSIONS

In summary, we have proposed a band alignment model that determines the morphology of the electrochemically deposited semiconductor layer on the semiconducting nanoporous oxide electrode. The electron microscopy combined with a photoelectrochemical measurement revealed that the semiconductor forms conformal coating on the electrode surface when its conduction band is higher than that of the electrode (e.g., CdSe/TiO_2 system). On the other hand, the semiconductor fills the pores of the electrode completely in the case of the opposite band offset. The amorphous as-deposited CdSe conformal layer crystallized to the hexagonal wurtzite phase after annealing at 400 °C for 1 h under a N_2 atmosphere. The CdSe-sensitized TiO_2 NT electrode exhibited faster charge transport and slower charge recombination than the dye-sensitized counterpart. The band alignment model proposed in the study provides a convenient avenue of determining materials combination for the morphology control during the electrochemical deposition.

AUTHOR INFORMATION

Corresponding Authors

*E-mail: afrank@nrel.gov (A.J.F.).

DOI: 10.1021/acsomega.9b02552
ACS Omega 2019, 4, 19772−19776

*E-mail: jykmse@snu.ac.kr (J.Y.K.).

ORCID

Kai Zhu: 0000-0003-0908-3909

Jin Young Kim: 0000-0001-7746-9972

Notes

The authors declare no competing financial interest.

■ ACKNOWLEDGMENTS

This work was supported by the Basic Science Research Program (2017R1A2B3010474), Nano-Material Technology Development Program (2016M3A7B4909369), and the Creative Materials Discovery Program (2017M3D1A1039377) through the National Research Foundation of Korea (NRF) funded by the Ministry of Science and ICT. This work was also supported by the Korea Institute of Energy Technology Evaluation and Planning (KETEP), granted funded by the Ministry of Trade, Industry and Energy (MOTIE) of the Republic of Korea (No. 20194010000260).

■ REFERENCES

(1) Sharma, K.; Sharma, V.; Sharma, S. S. Dye-Sensitized Solar Cells: Fundamentals and Current Status. *Nanoscale Res. Lett.* **2018**, *13*, 381.

(2) Benesperi, I.; Michaels, H.; Freitag, M. The researcher's guide to solid-state dye-sensitized solar cells. *J. Mater. Chem. C* **2018**, *6*, 11903−11942.

(3) Pan, Z.; Rao, H.; Mora-Seró, I.; Bisquert, J.; Zhong, X. Quantum dot-sensitized solar cells. *Chem. Soc. Rev.* **2018**, *47*, 7659−7702.

(4) Song, J. H.; Jeong, S. Colloidal quantum dot based solar cells: from materials to devices. *Nano Convergence* **2017**, *4*, 21.

(5) Du, Z.; Artemyev, M.; Wang, J.; Tang, J. Performance improvement strategies for quantum dot-sensitized solar cells: a review. *J. Mater. Chem. A* **2019**, *7*, 2464−2489.

(6) Ali, N.; Hussain, A.; Ahmed, R.; Wang, M. K.; Zhao, C.; Haq, B. U.; Fu, Y. Q. Advances in nanostructured thin film materials for solar cell applications. *Renewable Sustainable Energy Rev.* **2016**, *59*, 726−737.

(7) Briscoe, J.; Dunn, S. Extremely thin absorber solar cells based on nanostructured semiconductors. *Mater. Sci. Technol.* **2011**, *27*, 1741−1756.

(8) Premaratne, K.; Akuranthilaka, S. N.; Dharmadasa, I. M.; Samantilleka, A. P. Electrodeposition using non-aqueous solutions at 170 °C and characterisation of CdS, CdSxSe(1−x) and CdSe compounds for use in graded band gap solar cells. *Renewable Energy* **2004**, *29*, 549−557.

(9) Wang, H.; Zhou, H.; Lu, J.; Yao, S.; Zhang, W. Electrodeposition of CdSe/TiO_2 Coaxial Nanocables for Enhanced Photocatalytic Performance and H_2 Evolution in Visible Light. *J. Electrochem. Soc.* **2018**, *165*, D160−D166.

(10) Ojo, A. A.; Dharmadasa, I. M. 15.3% efficient graded bandgap solar cells fabricated using electroplated CdS and CdTe thin films. *Sol. Energy* **2016**, *136*, 10−14.

(11) Seo, S. W.; Jeon, J.-O.; Seo, J. W.; Yu, Y. Y.; Jeong, J.-h.; Lee, D.-K.; Kim, H.; Ko, M. J.; Son, H. J.; Jang, H. W.; Kim, J. Y. Compositional and Interfacial Modification of $Cu_2ZnSn(S,Se)_4$ Thin-Film Solar Cells Prepared by Electrochemical Deposition. *ChemSusChem* **2016**, *9*, 439−444.

(12) Manzano, C. V.; Bürki, G.; Pethö, L.; Michler, J.; Philippe, L. Determining the diffusion mechanism for high aspect ratio ZnO nanowires electrodeposited into anodic aluminum oxide. *J. Mater. Chem. C* **2017**, *5*, 1706−1713.

(13) Seabold, J. A.; Shankar, K.; Wilke, R. H. T.; Paulose, M.; Varghese, O. K.; Grimes, C. A.; Choi, K.-S. Photoelectrochemical Properties of Heterojunction CdTe/TiO_2 Electrodes Constructed Using Highly Ordered TiO_2 Nanotube Arrays. *Chem. Mater.* **2008**, *20*, 5266−5273.

(14) Wang, Q.; Zhu, K.; Neale, N. R.; Frank, A. J. Constructing Ordered Sensitized Heterojunctions: Bottom-Up Electrochemical Synthesis of p-Type Semiconductors in Oriented n-TiO_2 Nanotube Arrays. *Nano Lett.* **2009**, *9*, 806−813.

(15) Edley, M. E.; Li, S.; Guglietta, G. W.; Majidi, H.; Baxter, J. B. Ultrafast Charge Carrier Dynamics in Extremely Thin Absorber (ETA) Solar Cells Consisting of CdSe-Coated ZnO Nanowires. *J. Phys. Chem. C* **2016**, *120*, 19504−19512.

(16) Major, J. D.; Tena-Zaera, R.; Azaceta, E.; Bowen, L.; Durose, K. Development of ZnO nanowire based CdTe thin film solar cells. *Sol. Energy Mater. Sol. Cells* **2017**, *160*, 107−115.

(17) Zhu, K.; Neale, N. R.; Miedaner, A.; Frank, A. J. Enhanced Charge-Collection Efficiencies and Light Scattering in Dye-Sensitized Solar Cells Using Oriented TiO2Nanotubes Arrays. *Nano Lett.* **2007**, *7*, 69−74.

(18) Nelson, J. J.; Amick, T. J.; Elliott, C. M. Mass Transport of Polypyridyl Cobalt Complexes in Dye-Sensitized Solar Cells with Mesoporous TiO_2 Photoanodes. *J. Phys. Chem. C* **2008**, *112*, 18255−18263.

(19) Lee, H. J.; Yum, J.-H.; Leventis, H. C.; Zakeeruddin, S. M.; Haque, S. A.; Chen, P.; Seok, S. I.; Grätzel, M.; Nazeeruddin, M. K. CdSe Quantum Dot-Sensitized Solar Cells Exceeding Efficiency 1% at Full-Sun Intensity. *J. Phys. Chem. C* **2008**, *112*, 11600−11608.

(20) Feng, X.; Zhu, K.; Frank, A. J.; Grimes, C. A.; Mallouk, T. E. Rapid Charge Transport in Dye-Sensitized Solar Cells Made from Vertically Aligned Single-Crystal Rutile TiO_2 Nanowires. *Angew. Chem., Int. Ed.* **2012**, *51*, 2727−2730.

(21) Löher, T.; Jaegermann, W.; Pettenkofer, C. Formation and electronic properties of the CdS/$CuInSe_2$ (011) heterointerface studied by synchrotron-induced photoemission. *J. Appl. Phys.* **1995**, *77*, 731−738.

(22) Grätzel, M. Photoelectrochemical cells. *Nature* **2001**, *414*, 338−344.

(23) Wang, C.; Shim, M.; Guyot-Sionnest, P. Electrochromic Nanocrystal Quantum Dots. *Science* **2001**, *291*, 2390−2392.

(24) Kim, J.; Choi, S.; Noh, J.; Yoon, S.; Lee, S.; Noh, T.; Frank, A. J.; Hong, K. Synthesis of CdSe−TiO_2 Nanocomposites and Their Applications to TiO2 Sensitized Solar Cells. *Langmuir* **2009**, *25*, 5348−5351.

(25) Tena-Zaera, R.; Katty, A.; Bastide, S.; Lévy-Clément, C. Annealing Effects on the Physical Properties of Electrodeposited ZnO/CdSe Core−Shell Nanowire Arrays. *Chem. Mater.* **2007**, *19*, 1626−1632.

(26) Tiwana, P.; Docampo, P.; Johnston, M. B.; Snaith, H. J.; Herz, L. M. Electron Mobility and Injection Dynamics in Mesoporous ZnO, SnO_2, and TiO_2 Films Used in Dye-Sensitized Solar Cells. *ACS Nano* **2011**, *5*, 5158−5166.

(27) Preethi, L. K.; Antony, R. P.; Mathews, T.; Walczak, L.; Gopinath, C. S. A Study on Doped Heterojunctions in TiO_2 Nanotubes: An Efficient Photocatalyst for Solar Water Splitting. *Sci. Rep.* **2017**, *7*, 14314.

(28) Regonini, D.; Groff, A.; Sorarù, G. D.; Clemens, F. J. Photoelectrochemical study of anodized TiO_2 Nanotubes prepared using low and high H2O contents. *Electrochim. Acta* **2015**, *186*, 101−111.

(29) van de Lagemaat, J.; Frank, A. J. Nonthermalized Electron Transport in Dye-Sensitized Nanocrystalline TiO_2 Films: Transient Photocurrent and Random-Walk Modeling Studies. *J. Phys. Chem. B* **2001**, *105*, 11194−11205.

(30) Nelson, J.; Haque, S. A.; Klug, D. R.; Durrant, J. R. Trap-limited recombination in dye-sensitized nanocrystalline metal oxide electrodes. *Phys. Rev. B* **2001**, *63*, 205321.

(31) Frank, A. J.; Kopidakis, N.; Lagemaat, J. v. d. Electrons in nanostructured TiO_2 solar cells: transport, recombination and photovoltaic properties. *Coord. Chem. Rev.* **2004**, *248*, 1165−1179.

(32) van de Lagemaat, J.; Frank, A. J. Effect of the Surface-State Distribution on Electron Transport in Dye-Sensitized TiO_2 Solar Cells: Nonlinear Electron-Transport Kinetics. *J. Phys. Chem. B* **2000**, *104*, 4292−4294.

DOI: 10.1021/acsomega.9b02552
ACS Omega 2019, 4, 19772−19776